

Supporting Information: Spatially Heterogeneous Chlorine Incorporation in Organic-Inorganic Perovskite Solar Cells

*Yanqi Luo,^a Shany Gamliel,^b Sally Nijem,^b Sigalit Aharon,^b Martin Holt,^c Benjamin Stripe,^d
Volker Rose,^{c,d} Mariana I Bertoni,^e Lioz Etgar,^b and David P. Fenning^{a,*}*

^a, Department of Nanoengineering, University of California San Diego, La Jolla, CA 92093

^b The Institute of Chemistry, The Hebrew University of Jerusalem, Jerusalem, 91904, Israel

^c Center for Nanoscale Materials, Argonne National Laboratory, Argonne, IL 60439

^d Advanced Photon Source, Argonne National Laboratory, Argonne, IL 60439

^e School of Electrical, Computer and Energy Eng., Arizona State University, Tempe, AZ 85287

*E-mail: dfenning@ucsd.edu

1.1 X-ray beam resolution

A 50 nm wide Ti test pattern was used to analyze the X-ray beam's full width half maximum (FWHM). A horizontal line scan across the Ti pattern resulted in the Ti XRF profile shown in Fig S1 (open circles). A calculated convolution of the 50 nm Ti pattern with an assumed 90 nm FWHM beam spot results in a simulated Ti profile in excellent agreement with that experimentally measured (solid line, Fig S1).

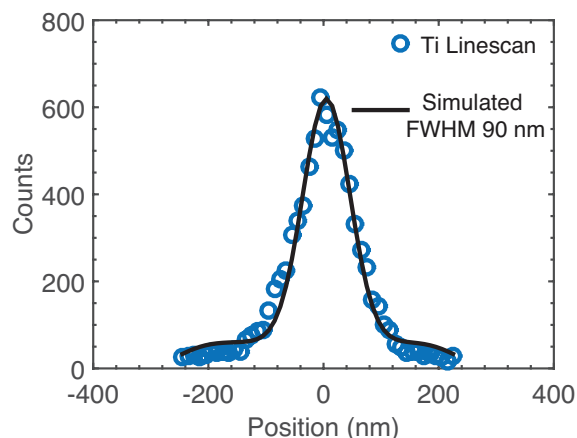


Fig S1 Ti X-ray fluorescence counts resulting from a scan of the X-ray beam across a 50 nm Ti test pattern (open circles). The convolution of the 50 nm pattern with an assumed 90 nm FWHM beam is overlaid (solid line).

1.2 XRD Measurement

X-ray powder diffraction measurements were performed in grazing incidence X-ray diffraction (GIXRD) mode on the D8 Advance Diffractometer (Bruker AXS, Karlsruhe, Germany) with a goniometer radius of 217.5 mm, a secondary graphite monochromator, 2° Soller slits and a 0.2 mm receiving slit. XRD patterns within the range 5° to 70° 2 θ were recorded at room temperature using CuK α radiation (λ 1.5418 Å) with the following measurement conditions: tube voltage of 40 kV, tube current of 40 mA, step-scan mode with a step size of 0.02° 2 θ and counting time of 1–3 s per step. The value of the grazing incidence angle was 2.5°. Fig S2 shows XRD spectra comparison between four different films and no residual MACl nor PbCl₂ has been detected.

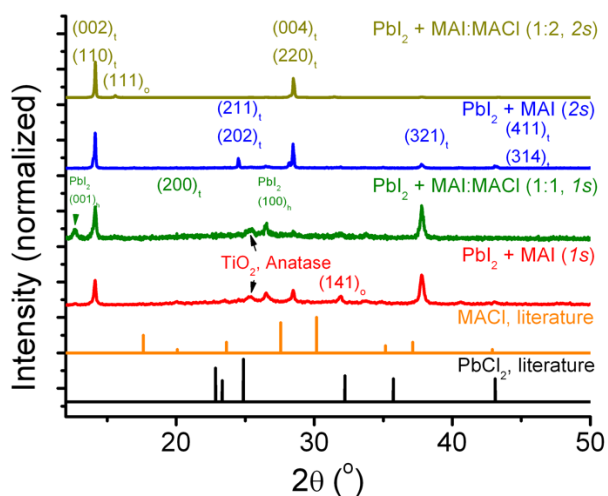


Fig S2. Four different films are analyzed by X-ray diffraction: PbI₂ + MAI:MACl (1:2, 2s), PbI₂ + MAI (2s), PbI₂ + MAI:MACl (1:1, 1s), and PbI₂ + MAI (1s). Reference standards for MACl and PbCl₂, from ICSD database collection

code 110647 and 43344 respectively, are shown. There is no indication of residual MgCl_2 nor PbCl_2 precursor when comparing films synthesized using chlorine-containing precursor and the ones with chlorine-free precursors regardless of the deposition process.

1.3 Film Stability under 10 keV X-Ray Beam

The spatial distribution and composition of the films were confirmed to be stable under the focused 10 keV X-ray illumination with 4×10^8 photons/sec on the 100 nm length scale of measurement by scanning with a 50 nm step size three times consecutively over the same area for a total period of three hours as shown in Figure S3. In this case, a Br:I mixture was used. Methylammonium bromide was obtained via the same synthesis route as MAI but with 1:1.5 mass ratio of methylamine to hydrobromic acid (HBr, 48 % in water, Sigma Aldrich). This film was synthesized via 2s deposition method. The three sequential XRF maps were registered to account for thermal drift. The thermal drift is less than 200 nm/hr. Fig S3 displays the three iodine XRF maps of the region of interest over time and, above, a histogram displays the iodine concentration distribution within the sample. The distributions are centered around $1100 \mu\text{g}/\text{cm}^2$ and no significant variation is observed on the histograms, suggesting the perovskite films are chemically stable under the hard x-ray incident beam in the given flux. This quantitative signal is obtained by normalizing the raw signal against the signal of a known concentration standard. (RF8-200-S2455, Thin Film XRF Reference Sample, AXO DRESDEN GmbH). All the perovskite films reported here were coated with a thin Au layer, which appears to help prevent degradation presumably due to providing an “encapsulation” effect, improved thermal transport, and/or X-ray excited carrier transport.

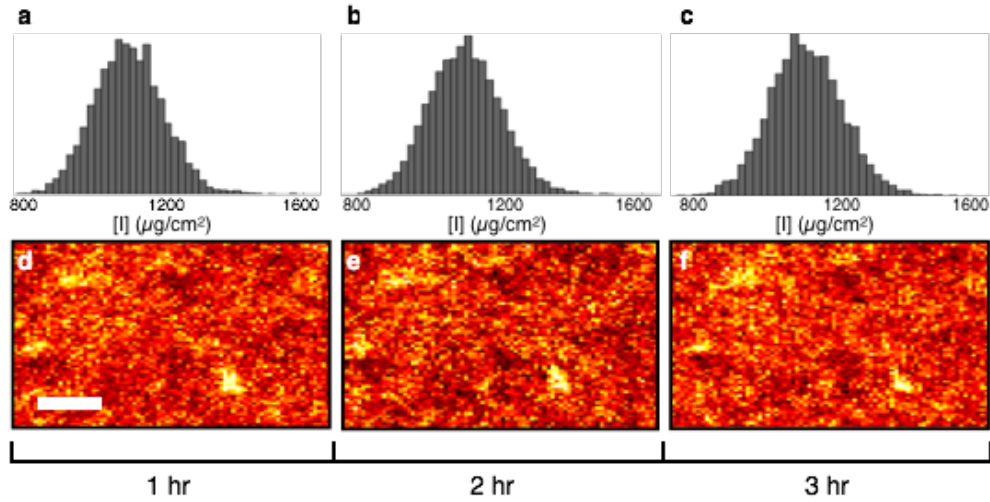


Fig S3. Repeated iodine X-ray fluorescence mappings under hard x-ray illumination over 3 hours (scale bar, $1 \mu\text{m}$). The histogram above each XRF map shows the corresponding distribution of iodine concentration in $\mu\text{g}/\text{cm}^2$. The mean and standard deviation for histogram a, b and c are $\mu_a=1099.2 \mu\text{g}/\text{cm}^2$, $\sigma_a=102.2 \mu\text{g}/\text{cm}^2$, $\mu_b=1102.3 \mu\text{g}/\text{cm}^2$, $\sigma_b=101.6 \mu\text{g}/\text{cm}^2$, $\mu_c=1101.9 \mu\text{g}/\text{cm}^2$, and $\sigma_c=99.3 \mu\text{g}/\text{cm}^2$.

1.4 Film Normalization to Account for Au and Film Thickness

To quantify the XRF signal, it is important to consider the signal attenuation within Au current collector overlayer and the film self-absorption. According to Beer Lambert’s law, the attenuation of light intensity within a medium is expressed as:

$$I = I_0 \exp\left(\frac{-t}{\lambda_i \cos \alpha}\right); \quad (1)$$

where I_0 is the incident intensity of light, λ_i is the attenuation length of incident X-rays, t is depth and α is incident angle with respect to the sample normal. We assume the element-specific attenuation factor a_y is proportional to overall attenuation of fluorescent photons that are collected by the finite solid angle swept by a detector at an angle β to the sample normal, which can be expressed as a function of film thickness,

$$a_y(t) \propto \int_0^t \exp\left(\frac{-t}{\lambda_i \cos \alpha}\right) \exp\left(\frac{-t}{\lambda_{o-y} \cos \beta}\right) \exp\left(\frac{-t_{Au}}{\lambda_{i-Au} \cos \alpha}\right) \exp\left(\frac{-t_{Au}}{\lambda_{o-Au} \cos \beta}\right) dt \quad (2)$$

where λ_o is element-specific fluorescence attenuation length, t is the thickness of perovskite absorber and t_{Au} is the thickness of Au current collector overlayer. Then the overall element-specific attenuation factor a_y is:

$$a_y(t) \propto \frac{\lambda_i \lambda_{o-y} \cos \alpha \cos \beta}{(\lambda_{o-y} \cos \beta + \lambda_i \cos \alpha)} \exp\left(-t \frac{\lambda_{o-Au} \cos \beta + \lambda_{i-Au} \cos \alpha}{\lambda_{i-Au} \lambda_{o-Au} \cos \beta \cos \alpha}\right) \left(1 - \exp\left(-t \frac{(\lambda_{o-y} \cos \beta + \lambda_i \cos \alpha)}{\lambda_i \lambda_{o-y} \cos \alpha \cos \beta}\right)\right) \quad (3)$$

The effective attenuation length for the incident 10keV X-ray beam in the perovskite film is 11.69 μm at 60° to detector. The overall attenuation of fluorescent photons for Pb, I, and Cl are 0.36, 0.51, and 0.32 for the 1 μm spray-deposited film; and 0.17, 0.22, and 0.16 respectively for the 300 nm films from 1s and 2s deposition. The error of Cl:I ratio is small due to thickness variation. The error due to a variation of 10% in film thickness is calculated to be around 0.7%.

1.5 Determination of Film Coverage on TiO_2 substrate

The Ti:I XRF response is used to automatically threshold where the film covers the substrate. High Ti:I ratio indicates poor film coverage, while low Ti:I ratio suggests relatively better perovskite film coverage areas. A cutoff at the arithmetic mean of Ti:I ratio plus three standard deviations was used. Fig S4 shows an example comparison of between original an XRF iodine map and after film coverage determination.

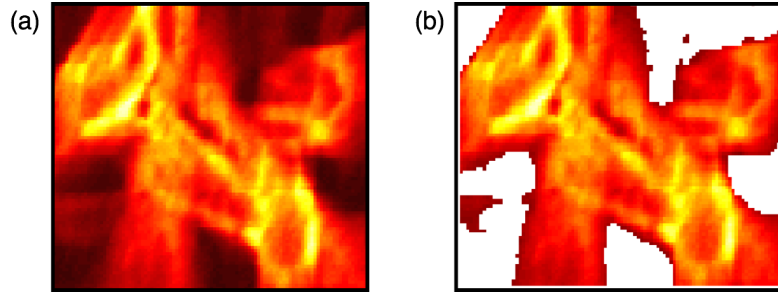


Figure S4. Example of film determination from XRF iodine map. To select the area of interest, we use the mean of Ti:I ratio combining with its standard deviation of each corresponding sample as the threshold limit (a) XRF iodine map of sample $\text{PbCl}_2 + \text{MAI}$ (1s) (b) Selected areas after threshold limit.

1.6 Quantitative data before normalization

Quantified data of individual I and Cl elemental response in $\mu\text{g}/\text{cm}^2$ is shown in Figure S5. The quantified loadings resulting from fitting of the I_L and $Cl_{K\alpha}$ fluorescence are shown. In our analysis, we focus on the quantitative Cl:I ratio, as shown in the third column below. The Cl:I data of Fig. 3 show the same Cl:I data, but with identical color scaling from Cl:I 0.0 to 0.12. Each sample's Cl:I is shown on its own scale below. The theoretical fluorescence yield of the Pb_M line resulted in an unreliable fit, and the Pb map of Fig. 3 is for qualitative comparison only.

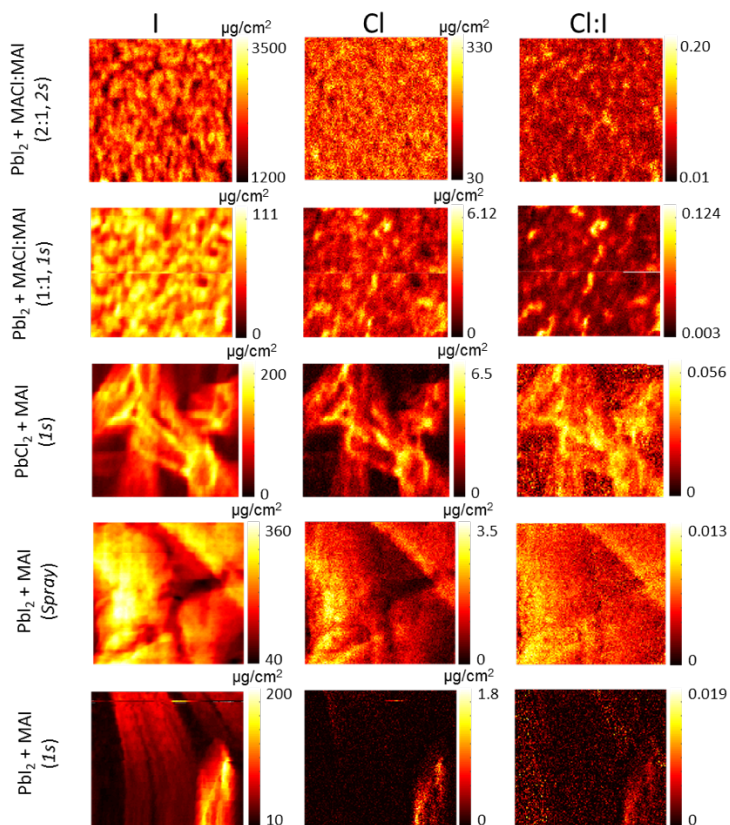


Figure S5. Quantified I and Cl concentration within samples along with the corresponding halide ratio map.

1.7 Single Particle Selection from XRF Maps

After using the Ti:I ratio to choose the film coverage area, this selected area map is further used to assist single-particle selection and isolation. The selection of individual particles is accomplished using MATLAB's built in watershed method to identify particles.